Draft version March 3, 2022
Typeset using LaTeX default style in AASTeX62

arXiv:1902.04824v1 [astro-ph.SR] 13 Feb 2019

Diagnosing the Clumpy Protoplanetary Disk of the UXor Type Young Star GM Cephei

P. C. Huang,[1] W. P. Chen,[1,2] M. Mugrauer,[3] R. Bischoff,[3] J. Budaj,[4] O. Burkhonov,[5] S. Ehgamberdiev,[5] R. Errmann,[6,7] Z. Garai,[4] H. Y. Hsiao,[1] C. L. Hu,[8] R. Janulis,[9] E. L. N. Jensen,[10] S. Kiyota,[11] K. Kuramoto,[12] C. S. Lin,[1] H. C. Lin,[1] J. Z. Liu,[13] O. Lux,[3] H. Naito,[14] R. Neuhäuser,[3] J. Ohlert,[15,16] E. Pakštienė,[17] T. Pribulla,[4] J. K. T. Qvam,[18] St. Raetz,[19,20] S. Sato,[21] M. Schwartz,[22] E. Semkov,[23] S. Takagi,[12] D. Wagner,[3] M. Watanabe,[24] and Yu Zhang[13]

[1] *Graduate Institute of Astronomy, National Central University, 300 Zhongda Road, Zhongli, Taoyuan 32001, Taiwan*
[2] *Department of Physics, National Central University, 300 Zhongda Road, Zhongli, Taoyuan 32001, Taiwan*
[3] *Astrophysikalisches Institut und Universitäts-Sternwarte, FSU Jena, Schillergäßchen 2-3, D-07745 Jena, Germany*
[4] *Astronomical Institute, Slovak Academy of Sciences, 059 60 Tatranská Lomnica, Slovak Republic*
[5] *Ulugh Beg Astronomical Institute of the Uzbek Academy of Sciences, 33 Astronomicheskaya str., Tashkent 100052, Uzbekistan*
[6] *Centre for Astrophysics Research (CAR), University of Hertfordshire, Hatfield Hertfordshire, AL10 9AB,UK*
[7] *Abbe Center of Photonics, Friedrich-Schiller-Universität Jena, Max-Wien-Platz 1, D-07743 Jena, Germany*
[8] *Taipei Astronomical Museum, 363 Jihe Road, Shilin, Taipei 11160, Taiwan*
[9] *Institute of Theoretical Physics and Astronomy, Vilnius University, Saulėtekio av. 3, 10257 Vilnius, Lithuania*
[10] *Department of Physics and Astronomy, Swarthmore College, 500 College Avenue, Swarthmore, PA 19081, USA*
[11] *Variable Stars Observers League in Japan (VSOLJ), 7-1 Kitahatsutomi, Kamagaya, Chiba 273-0126, Japan*
[12] *Department of Cosmosciences, Hokkaido University, Kita 10, Nishi 8, Kita-ku, Sapporo, Hokkaido 060-0810, Japan*
[13] *National Astronomical Observatories, Xinjiang Observatory, Chinese Academy of Sciences, 150, Science 1-Street, Urumqi, Xinjiang 830011, China*
[14] *Nayoro Observatory, 157-1 Nisshin, Nayoro, Hokkaido 096-0066, Japan*
[15] *University of Applied Sciences, Wilhelm-Leuschner-Strasse 13, D-61169 Friedberg, Germany*
[16] *Michael Adrian Observatory, Astronomie Stiftung Trebur, Fichtenstrasse 7, D-65468 Trebur, Germany*
[17] *Institute of Theoretical Physics and Astronomy, Vilnius University, Saulėtekio av. 3, 10257 Vilnius, Lithuania*
[18] *Department of Physics, University of Oslo, P.O. Box 1048 Blindern, NO-0316 Oslo, Norway*
[19] *Freiburg Institute of Advanced Studies (FRIAS), University of Freiburg, Albertstraße 19, D-79104 Freiburg, Germany*
[20] *Institute for Astronomy and Astrophysics Tübingen (IAAT), University of Tübingen, Sand 1, D-72076 Tübingen, Germany*
[21] *Astrophysics Department, Nagoya University, Nagoya, 464-8602, Japan*
[22] *Tenagra Observatory, 221 Calle Coco, Rio Rico, AZ 85648, USA*
[23] *Institute of Astronomy and National Astronomical Observatory, Bulgarian Academy of Sciences, 72 Tsarigradsko Shosse Blvd., 1784 Sofia, Bulgaria*
[24] *Department of Applied Physics, Okayama University of Science 1-1 Ridai-cho, Kita-ku, Okayama, Okayama 700-0005, Japan*

Submitted to ApJ

ABSTRACT

UX Orionis stars (UXors) are Herbig Ae/Be or T Tauri stars exhibiting sporadic occultation of stellar light by circumstellar dust. GM Cephei is such a UXor in the young ($\sim$ 4 Myr) open cluster Trumpler 37, showing prominent infrared excess, emission-line spectra, and flare activity. Our photometric monitoring (2008–2018) detects (1) an $\sim$3.43 day period, likely arising from rotational modulation by surface starspots, (2) sporadic brightening on time scales of days due to accretion, (3) irregular minor flux drops due to circumstellar dust extinction, and (4) major flux drops, each lasting for a couple of months with a recurrence time, though not exactly periodic, of about two years. The star experiences normal reddening by large grains, i.e., redder when dimmer, but exhibits an unusual "blueing" phenomenon in that the star turns blue near brightness minima. The maximum extinction during relatively short (lasting $\leq$ 50 days) events, is proportional to the duration, a consequence of varying clump

Corresponding author: P. C. Huang
pochiehhuang1@gmail.com

sizes. For longer events, the extinction is independent of duration, suggestive of a transverse string distribution of clumps. Polarization monitoring indicates an optical polarization varying $\sim$ 3%–8%, with the level anticorrelated with the slow brightness change. Temporal variation of the unpolarized and polarized light sets constraints on the size and orbital distance of the circumstellar clumps in the interplay with the young star and scattering envelope. These transiting clumps are edge-on manifestations of the ring- or spiral-like structures found recently in young stars with imaging in infrared of scattered light, or in submillimeter of thermalized dust emission.

Keywords: circumstellar matter — occultations — protoplanetary disks — stars: individual (GM Cephei) — stars: pre-main sequence — stars: variables: T Tauri, Herbig Ae/Be

1. INTRODUCTION

Circumstellar environments are constantly changing. A young stellar object (YSO), with prominent chromospheric and coronal activities, interacts intensely with the surrounding accretion disk by stellar/disk winds and outflows. The first few million years of the pre-main-sequence (PMS) evolution coincide with the epoch of possible planet formation, during which grain growth, already taking place in prestellar molecular cores up to micron sizes, continues on to centimeter sizes, and then to planetesimals (Natta et al. 2007). The detailed mechanism to accumulate planetesimals and to eventual planets is still uncertain. Competing theories include planetesimal accretion (Weidenschilling 2000) versus gravitational instability (Safronov 1972; Goldreich & Ward 1973; Johansen et al. 2007). Given the ubiquity of exoplanets, planet formation must be efficient to complete with the dissipation of PMS optically thick disks in less than 10 Myr (Mamajek et al. 2004; Briceño et al. 2007; Hillenbrand 2008).

YSOs are known to vary in brightness. Outbursts arising from intermittent mass accretion events are categorized into two major classes: (1) FU Ori-type stars (or FUors) showing erupt brightening up to 6 mag from quiescent to the high state in weeks to months, followed by a slow decline in decades (Hartmann & Kenyon 1985), and (2) EX Lup-type stars (EXors) showing brightening up to 5 mag, sometimes recurrent, with roughly the same timescale of months in both rising and fading (Herbig 1989). Sunlike PMS objects, i.e., T Tauri stars, may also display moderate variations in brightness and colors (Herbst et al. 1994) due to rotational modulation by magnetic/chromospheric cool spots or accretion/shocking hot spots on the surface. There is an additional class, owing its variability to extrinsic origin, of UX Ori type stars (UXors; Herbst et al. 1994), that displays irregular dimming caused by circumstellar dust extinction. In addition to the prototype UX Ori itself, examples of UXors include CO Ori, RR Tau, and VV Ser.

The YSO dimming events can be further categorized according to the levels of extinction and the timescales. The "dippers" (Cody & Hillenbrand 2010), with AA Tau being the prototype (Bouvier et al. 1999, 2003), have short (1–5 days) and quasi-periodic events thought to originate from occultation by warps (Terquem & Papaloizou 2000; Cody et al. 2014) or by funnel flows (Blinova et al. 2016) near the disk truncation radius and induced by the interaction between the stellar magnetosphere and the inner disk (Romanova et al. 2013). The "faders," with KH 15D being the prototype (Kearns & Herbst 1998; Hamilton et al. 2001), show prolonged fading events, each lasting for months to years with typically large extinction up to several magnitudes, thought to be caused by occultation by the outer part of the disk (Bouvier et al. 2013; Rodriguez et al. 2015, 2016). The target of this work, GM Cephei (hereafter GM Cep), a UXor star known to have a clumpy dusty disk (Chen et al. 2012), displays both dipper and fader events.

As a member of Trumpler (Tr) 37, a young (1–4 Myr, (Marschall et al. 1990; Patel et al. 1995; Sicilia-Aguilar et al. 2005; Errmann et al. 2013)) star cluster as a part of the Cepheus OB2 association, GM Cep (R.A.=$21^{\rm h}38^{\rm m}17\overset{\rm s}{.}32$, Decl.=$+57°31'22''$, J2000) possesses observational properties typical of a T Tauri star, such as emission spectra, infrared excess, and X-ray emission (Sicilia-Aguilar et al. 2008; Mercer et al. 2009). *Gaia*/DR2 (Gaia Collaboration et al. 2018) measured a parallax of $\varpi = 1.21 \pm 0.02$ mas ($d = 826^{+14}_{-13}$ pc), consistent with being a member of Tr 37 at $\sim$ 870 pc (Contreras et al. 2002).

The spectral type of GM Cep reported in the literature ranges from a late F (Huang et al. 2013) to a late G or early K (Sicilia-Aguilar et al. 2008). The star has been measured to have a disk accretion rate up to $10^{-6} M_\odot$ yr^{-1}, which is thought to be 2–3 orders higher than the median value of the YSOs in Tr 37 and is 1–2 orders higher than those of typical T Tauri stars (Gullbring et al. 1998; Sicilia-Aguilar et al. 2008). The broad spectral lines suggest a rotation $v \sin i \sim 43.2$ km s^{-1} much faster than the average $v \sin i \sim 10.2$ km s^{-1} of the members of Tr 37 (Sicilia-Aguilar et al. 2008).

Sicilia-Aguilar et al. (2008) presented a comprehensive collection of data on GM Cep, including optical/infrared photometry and spectroscopy, plus millimeter line and continuum observations, along with the young stellar population in the cluster Tr 37 and the Cep OB2 association (See also Sicilia-Aguilar et al. 2004, 2005, 2006a,b). Limited by the time span of their light curve, Sicilia-Aguilar et al. (2008) made the incorrect conclusion that the star belonged to the EXor type. Later, with a century-long light curve derived from archival photographic plates, covering 1895 to 1993, Xiao et al. (2010) classified the star as a UXor, which was confirmed by subsequent intense photometric monitoring (Chen et al. 2012; Semkov & Peneva 2012; Semkov et al. 2015; Huang et al. 2018). Chen et al. (2012) speculated on a possible recurrent time of ~ 1 yr based on a few major brightness dimming events, but this was not substantiated by Semkov et al. (2015).

GM Cep has been studied as a part of the Young Exoplanet Transit Initiative (YETI) project (Neuhäuser et al. 2011), which combines a network of small telescopes in distributed time zones to monitor young star clusters, with the goal to find possible transiting exoplanets (Neuhäuser et al. 2011). Any exoplanets thus identified would have been newly formed or in the earliest evolution, providing a comparative sample with the currently known exoplanets that are almost exclusively found in the general Galactic fields, so are generally older). While so far YETI has detected only exoplanet candidates (Garai et al. 2016; Raetz et al. 2016), the data set serves as a valuable inventory for studies such as stellar variability (Errmann et al. 2013; Fritzewski et al. 2016).

The work reported here includes light curves in BVR bands on the basis of the photometry collected from 2008 to 2018. Moreover, polarization measurements in g'-, r'-, and i'-bands have been taken at different brightness phases, enabling simultaneous photometric and polarimetric diagnosis of the properties of the circumstellar dust clumps that cause the UXor variability. §2 summarizes the data used in this study, including those collected in the literature, and our own photometric and polarimetric observations. §3 presents the results of photometric, color, and polarimetric variations. On the temporal behavior of these measurements, we then discuss in §4 the implications on the properties of the dust clumps around GM Cep. We summarize our findings in §5.

2. DATA SOURCES AND OBSERVATIONS

Optical data of GM Cep consist mostly of our own imaging photometry since mid-2008, and polarimetry since mid-2014, up to mid-2018. These are supplemented by data adopted from the American Association of Variable Star Observers (AAVSO) database, covering timescales from days/weeks to years. Sicilia-Aguilar et al. (2008) summarized the photometry from the literature, e.g., those of Morgenroth (1939) Suyarkova (1975), and Kun (1986), and from databases such as VizieR, SIMBAD, and SuperCOSMOS (Monet et al. 2003), along with the infrared data from *IRAS* and MSX6C. Xiao et al. (2010) expanded the light-curve baseline and presented a-century-long photometric measurements, with a photometric uncertainty of ~ 0.15 mag, derived from the photographic plates collected at the Harvard College Observatory and from Sonneberg Observatory. Previous optical monitoring data include those reported by Chen et al. (2012, in BVR covering end of 2009 to 2011), by Semkov & Peneva (2012), and by Semkov et al. (2015, in $UBVRI$ to end of 2014). The AAVSO data were adopted only from the observer "MJB" after checking photometric consistency with our results.

2.1. *Optical photometry*

The imaging photometry covering 10 years has been acquired by 16 telescopes, including seven of the YETI telescopes (Neuhäuser et al. 2011). The Tenagra Observatory in Arizona and Lulin Observatory in Taiwan contributed about four-year baseline coverage each from mid-2010 to mid-2018, respectively. The Tenagra II telescope, a 0.81m, Ritchey–Chrétien type telescope, carried out the BVR monitoring from 2010 October to 2014 June. No observations were taken in July/August because of the monsoon season, or during February/March because of the invisibility of the target. The SLT 0.4 m telescope, located at Lulin Observatory, acquired a few data points in BVR bands every night from 2014 September to date, weather permitting. Technical parameters of additional telescopes contributing to the data are listed in Table 1.

For each observing session, darks and bias frames were obtained every night when science frames were taken, except for the STK and CTK-II, for which darks already include biases. The sky flats were obtained when possible. For those nights without sky flats, we used the flats from the nearest previous night. The standard reduction with dark, bias, and flat field correction was performed with IRAF. For the Maidanak Observatory, Nayoro Observatory, and the ESA's OGS, the images were only corrected with bias and flat because of the low temperatures of the CCD detectors used.

Table 1. Parameters of Telescopes

Observatory/Telescope	CCD Type	Size (pixels)	Pixel Size (μm)	FOV (arcmin^2)	RON (e^-)	# Nights
YETI Telescopes						
0.4 m SLT (Lulin)	E2V 42-40	2048×2048	13.5	30.0×30.0	7	541
0.81 m TenagraII (Tenagra)	SITe SI-03xA	1024×1024	24	14.8×14.8	29	463
0.25 m CTK-II (Jena)[a]	E2V PI47-10	1056×1027	13	21.0×20.4	7	104
0.6 m STK (Jena)[b]	E2V 42-10	2048×2048	13.5	52.8×52.8	8	79
1.0 m LOT (Lulin)	Apogee U42	2048×2048	13.5	11.0×11.0	12	48
0.61 m RC (Van de camp)	Apogee U16M	4096×4096	9	26.0×26.0	7	13
0.6 m Zeiss 600/7500 (Stara Lesna)	FLI ML 3041	2048×2048	15	14.0×14.0	5	11
Other Telescopes						
1.6 m Pirka (Nayoro)[c]	EMCCD C9100-13	512×512	16	3.3×3.3	13	133
1.5 m AZT-22 (Maidanak)	SI 600 Series	4096×4096	15	16.0×16.0	5	120
1.0 m NOWT (XinJiang)	E2V 203-82	4096×4096	12	78.0×78.0	5	108
1.2 m T1T (Michael Adrian)	SBIG STL-6303	3072×2048	9	10.0×6.7	15	12
0.51 m CDK (Mayhill)	FLI ProLine PL11002M	4008×2072	9	36.2×54.3	9	12
1.0 m ESA's OGS (Teide)[d]	Roper Spec Camera	2048×2048	13.5	13.76×13.76	8	10
1.5 m P60 (Palomar)	AR-Coated Tektronix	2048×2048	24	11.0×11.0	9	7
0.35 m ACT-452 (MAO)	QSI 516	1552×1032	9	37.6×25.0	15	2

NOTE— [a]Mugrauer (2016); [b]Mugrauer & Berthold (2010); [c]Nayoro observatory equips EMCCD camera with their Multi-Spectral Imager (MSI) instrument(Watanabe et al. 2012); [d]Schulz et al. (2014).

Table 2. Photometric reference stars adopted from Xiao et al. (2010)

Refe Star	R.A. (J2000) (deg)	Decl. (J2000) (deg)	B (mag)	V (mag)	R (mag)
Star B	324.529226	57.508117	16.015	14.961	14.364
Star C	324.563184	57.492816	15.445	14.837	14.455
Star D	324.543391	57.505287	15.333	14.357	13.770
Star F	324.586443	57.487231	14.389	13.358	12.770
Star G	324.600939	57.556202	13.374	12.829	12.513

The brightness of GM Cep and photometric reference stars was each measured with the aperture photometry procedure "aper.pro" of IDL, which is similar to the "IRAF/Daophot" task, with an aperture radius of 8.″5 for the target, and an annulus of the inner radius of 9.″5 and outer radius of 13″for the sky. The seven reference stars from Xiao et al. (2010, their Table 2) were originally used by Chen et al. (2012), but later we found that Star A varied at ~ 0.1 mag level, and Star E was likely a member of the young cluster, so would be likely also variable. Excluding these two stars, the remaining five were used as reference stars in the differential photometry of GM Cep reported here.

Photometric measurements at multiple bands were taken at different epochs in a night, and sometimes with different telescopes. In order to facilitate a quantitative comparison, e.g., between the B- and V-band light curves, and hence the $B-V$ color curve, the epoch of each observation was rounded to the nearest integer Modified Julian Date (MJD), and the average in each band was taken within the same MJD. For periodicity analysis, the actual timing was used, so there would be no round-off error.

2.2. *Optical Polarimetry*

The optical polarization of GM Cep was measured by TRIPOL2, the second unit of the Triple-Range Imaging POLarimeter (TRIPOL, Chen et al. 2019, in preparation) attached to the LOT. This imaging polarimeter measures polarization in the Sloan g'-, r'-, and i'-bands simultaneously by rotating a half-wave plate to four angles, 0°, 45°, 22°.5, and 67°.5. To reduce the influence by sky conditions, every polarization measurement reported in this work was the mean value of at least fuve sets of images having nearly the same counts in each angle. This compromises the possibility to detect polarization variations on timescales of less than about an hour, but ensures the reliability of nightly measurements.

For TRIPOL2, we acquired the sky flats if weather allowed, or else we used the sky flats from the nearest adjacent night. Several unpolarized and polarized standard stars (Schmidt et al. 1992) were observed to calibrate the instrumental polarization and angle offset (Chen et al. 2019, in preparation). The correction for the dark and flat field was performed for all the images following the standard reduction procedure. The fluxes at four angles were measured with aperture photometry, and the Stokes parameters (I, Q, and U) were then calculated, from which the polarization percentage ($P = \sqrt{Q^2 + U^2}/I$) and position angle ($\theta = 0.5 \arctan(U/Q)^{-1}$) were derived. A typical accuracy $\Delta P \lesssim 0.3\%$ in polarization could be achieved in a photometric night (Chen et al. 2019, in preparation).

3. RESULTS AND DISCUSSIONS

3.1. *Photometric Variations*

Figure 1 exhibits the light curves of GM Cep, including data taken from the literature covering more than a century since 1895 (Figure 1a), and our intense multiband observations starting in 2008 (Figure 1b). Since last reported (Chen et al. 2012; Semkov & Peneva 2012; Semkov et al. 2015), the star continued to show abrupt brightness changes. There are three main kinds of variations. Most noticeable are the major flux drops, $\sim$ 1–2.5 mag at all B-, V-, and R-bands, with prominent ones, each lasting for months, occurring in mid-2009, mid-2010, 2011/2012, beginning of 2014, end of 2016, and end of 2017 (Munari et al. 2017). The list is not complete, limited by the time coverage of our observations. In addition, there are minor flux drops ($\sim$ 0.2–1 mag), each with the duration of days to weeks. The third kind, with a typical depth of 0.05 mag and occurring in a few days, is not discernible on the display scale of Figure 1, and will be discussed later.

3.1.1. *Periodicity Analysis*

Deep Flux Drops

The UXors are thought to have irregular extinction events, despite the attempts to search for cyclic variability (Grinin et al. 1998; Rostopchina et al. 1999). For GM Cep, period analysis by the Lomb–Scargle algorithm (Lomb 1976; Scargle 1982) was performed, and the result is shown in Figure 2. A significant power is seen at $\sim$ 730 days, which does not show up in the power spectrum of the sampling function (i.e., a constant magnitude at each sampling point). The secondary peak around 350 days, also visible in the sampling function, is the consequence of annual observing gaps. A dynamical period analysis was performed by repetitive Lomb–Scargle computation within a running window of 2,000 days with a moving step of one day. For example, the power spectrum at date 42500 (plus MJD+13000) was calculated by the data within the window ranging from 41500 to 43500. Enough padding was applied to the edges of the light curve. A peak around $\sim$ 700 days persists, evidenced in Figure 1c.

An independent investigation of the periodicity was performed by computing the autocorrelation function. The light curve was resampled to be equally spaced with a step of one day, and for each day, the average of data within 300 days from date 41500 to date 45500, or within 100 days from date 42300 to date 45500, centered on the day was adopted. A time lag of $\sim 700 - 800$ days is reaffirmed. This is the timescale between the few prominent minima (i.e., near 42900 and 43700).

Rotational Modulation

To investigate possible variability on much shorter time scales, we extracted the segment of the light curve from mid-2014 to the end of 2014, when the star was in the bright state so that there should be little influence by major flux drops. The light curve was fitted with, and then subtracted by, a third-order polynomial function to remove the slow-varying trend. The Lomb–Scargle analysis led to an identification of a period of $\sim$ 3.43 days in the detrended light curve, and Figure 3 exhibits the original and the detrended light curves, together with the power spectrum and the folded light curve. This variation is caused by modulation of stellar brightness by dark spots on the surface with the rotational period of the star (Strassmeier 2009). Note that this period coincides roughly with the expected rotational period of a few days for the star, given its measured rotation $v \sin i \sim 43$ km s^{-1}, and a radius of a few solar radii, estimated from the PMS evolutionary tracks (Sicilia-Aguilar et al. 2008).

Guided by the periodicity derived from the short segment of the light curve, we then processed the entire light curve using a more aggressive detrend technique than a polynomial fit to deal with the large fluctuations. The original light curve was smoothed by a running average, with an eight-day window. This effectively removes low-frequency signals slower than about 10 days. To investigate possible period changes, we divided the light curve into three segments, with the MJD ranges (plus MJD+13000) (1) 41500 to 43000, (2) 43000 to 44250, and (3) 44250 to 45500, respectively, based on a judicious choice to have sufficiently long trains of undersampled data to recover periods on time scales of

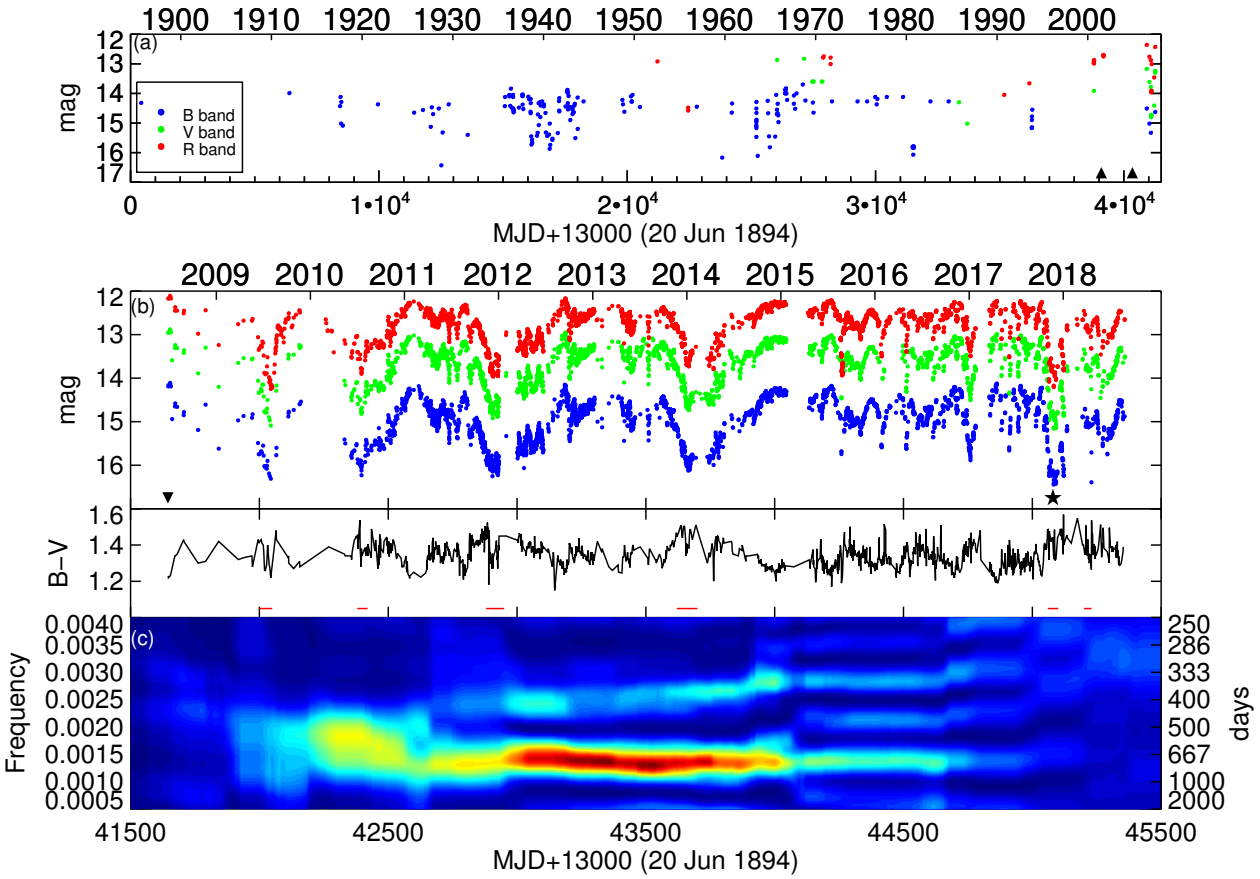


Figure 1. The light curve of GM Cep from 1894 to 2018. (a) The century-long data reported by Sicilia-Aguilar et al. (2008) and Xiao et al. (2010). (b) The light curves and $(B-V)$ color curve from 2008 to 2018 reported in this work. Epochs at which spectral measurements were reported in the literature are marked, with a triangle symbol for Sicilia-Aguilar et al. (2008), an upside down triangle for Semkov et al. (2015) and an asterisk for Giannini et al. (2018). (c) Dynamical period analysis of the input light curve of (b), with a window size of 2000 days and a step of 1 day. The color represents the power of the periodogram, from high in red to blue. The vertical axis represents either the frequency (on the left) or the corresponding period (right).

days. Figure 4 presents the power spectrum and the phased light curve for each segment, and in each case a significant period stands out, with the period and amplitude, $P_1 = 3.421$ days, $A_1 = 0.039$ mag $P_2 = 3.428$ days, $A_2 = 0.036$ mag, and $P_3 = 3.564$ days, $A_3 = 0.020$ mag. The seemingly large scattering in each folded light curve is not the noise in the data, but the intrinsic variation in the star's brightness, e.g., by differing total starspot areas. Because such a variation is not Gaussian, a least-squares analysis may not be appropriate to render a reliable estimate of the amplitude. Still, the sinusoidal behavior seems assured.

Therefore, a rotation period of roughly 3.43 days is found to persist throughout the entire time of our observations. Moreover there is marginal evidence of a lengthening period with a reduction in amplitude. This can be understood as latitudinal dependence of the occurrence of starspots due to surface differential rotation, in analog to the solar magnetic Schwabe cycle, in which sunspots first appear in heliographic mid-latitudes, and progressively more new sunspots turn up (hence covering a larger total surface) toward the equator (hence with shorting rotational periods). GM Cep therefore has an opposite temporal behavior, suggestive of an alternative dynamo mechanism at work (e.g.,

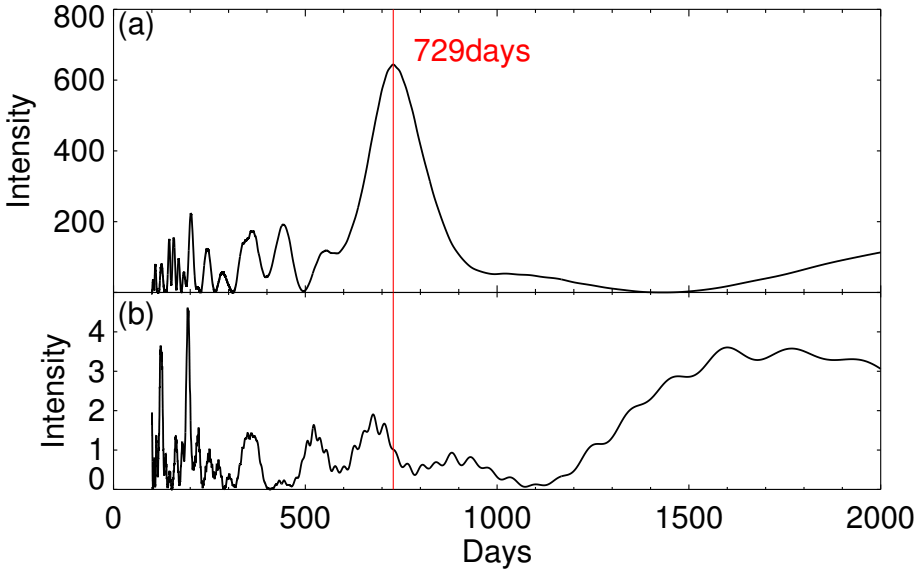


Figure 2. (a) The periodogram of the V-band light curve, where the red line marks the peak of the power spectrum. (b) The periodogram of the sampling function.

Küker et al. 2011). Further observations with a shorter cadence should be able to confirm this period shift and to provide a more quantitative diagnostic.

The detrended light curve shows mostly dimming events with occasional brightening episodes. The dimming must be the consequence of rotational modulation by surface starspots, whereas the brightening arises from sporadic accretion. The amplitude $\lesssim 0.2$ mag is consistent with the 0.01–0.5 mag variation range typically observed in T Tauri stars caused by cool or hot starspots (Herbst et al. 1994). Also, the amplitude of variation is marginally larger at shorter wavelengths, namely in V and B, lending evidence of accretion.

The excessive accretion rate of GM Cep reported by Sicilia-Aguilar et al. (2008), 10^{-7} to $5 \times 10^{-6} M_\odot$ yr^{-1}, was estimated by the U-band luminosity (Gullbring et al. 1998). Using the H$_\alpha$ velocity as an alternative diagnostic tool (Natta et al. 2004), the accretion rate would be 5×10^{-8} to $3 \times 10^{-7} M_\odot$ yr^{-1} (Sicilia-Aguilar et al. 2008). Similarly, measuring also the H$_\alpha$ velocity, Semkov et al. (2015) derived $1.8 \times 10^{-7} M_\odot$ yr^{-1}. Giannini et al. (2018) presented spectra of GM Cep at different brightness phases and, on the basis of the dereddened H$_\alpha$ luminosity and its relation to the accretion luminosity (Alcalá et al. 2017), and then to the accretion rate (Gullbring et al. 1998), derived an average accretion rate of $3.5 \times 10^{-8} M_\odot$ yr^{-1} with no significant temporal variations. Each of these methods has its limitation. The U-band flux may be contributed by thermal emission from the hot boundary layer (the accretion funnel) between the star and the disk. The H$_\alpha$ emission, on the other hand, may be contaminated by absorption in the H$_\alpha$ profile, or by chromospheric contribution not related to accretion. In any case, GM Cep does not seem to be unusually active in accretion activity compared to typical T Taur stars or Herbig Ae/Be stars. The prominent flux variations are the consequences of dust extinction, not the FUor kind of flares. In Figure 1(a) and (b), the epoches at which literature spectroscopic measurements are available are marked, at date 39091 (Sicilia-Aguilar et al. 2008) and at date 41645 (Semkov et al. 2015), both when the star was in a bright state, and at date $\sim$ 45080 (Giannini et al. 2018) when the star was in a faint state. Among the three datasets, the accretion rate does not seem to correlate with the apparent brightness.

3.1.2. *Event Duration and Extinction*

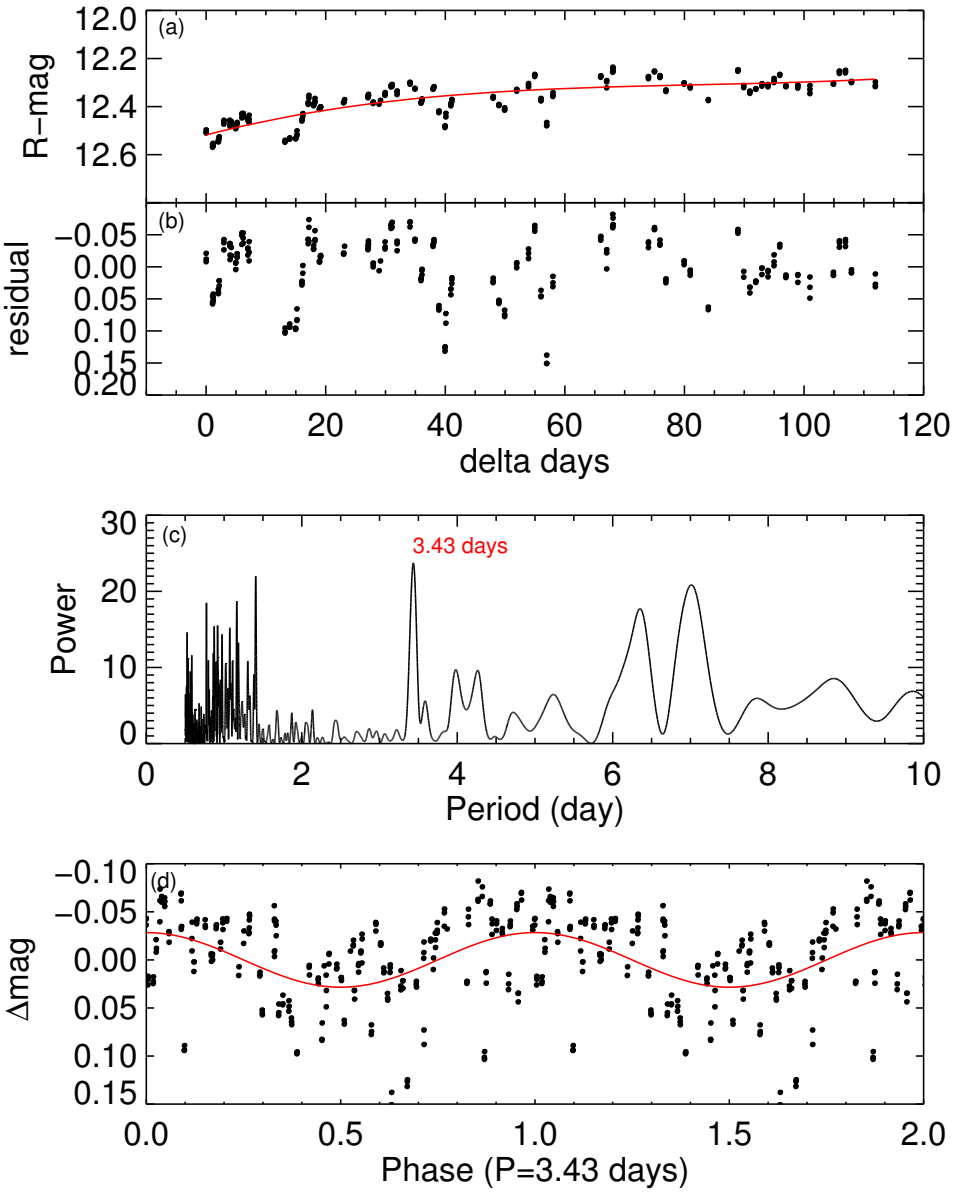


Figure 3. (a) The bright state in mid-2014 of the R-band light curve. (b) The scaled light curve after removal of the slow-varying trend. (c) The power spectrum of (b), from which a period of 3.43 days is detected. (d) The folded light curve with $P = 3.43$ days found in (c). The solid curve shows the best-fit sinusoidal function.

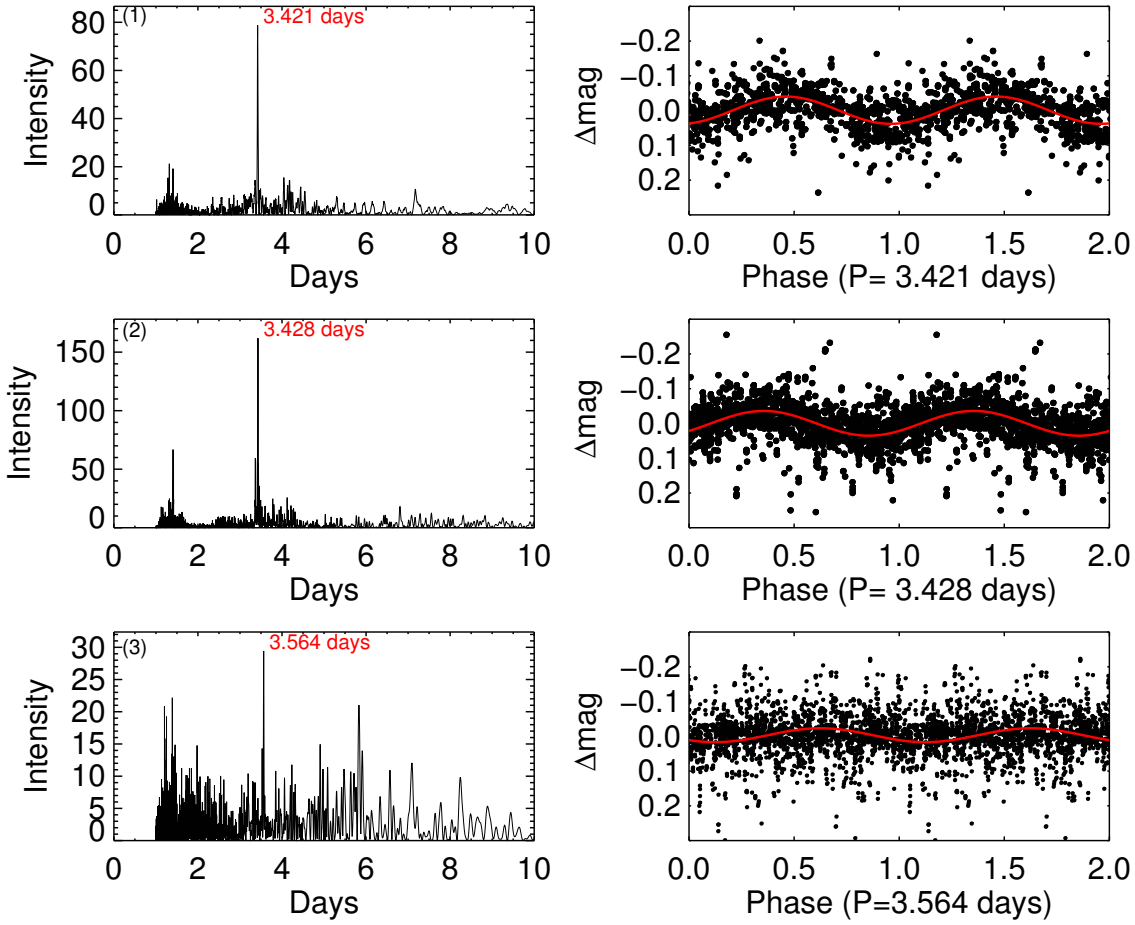


Figure 4. Power spectrum and phased light curve for (plus MJD+13000) (a) 41500–43000, (b) 43000–44250, and (3) 44250–45500. In each case the solid curve is the best-fit sinusoidal function, from which the amplitude is derived.

We parameterize a flux drop event by its duration and the maximum depth, with a least-squares fit by a Gaussian function. Only events sampled at more than half of the duration, e.g., an event lasting for roughly 10 days must have been observed for more than 5 nights, are considered to have sufficient temporal coverage to be included in the analysis. Figure 5 illustrates how the duration, taken as five times the standard deviation, or about 5% below the continuum, and the depth, as the minimum of the Gaussian function, are derived for each major event. The parameters are summarized in Table 3, in which the columns list for each event the identification, the MJD, duration, depths in B-, V- and R-bands, and the comments.

Figure 6 exhibits the duration versus depth of the flux drop events. Two distinct classes of events emerge. For the short events the duration in general lengthens with the depth, roughly amounting to $A_V \sim 1$ mag per 30 days. This is understood as the various sizes of occulting clumps, so a larger clump leads to a longer event along with a deeper minimum. The extinction depth levels off for longer ($\gtrsim 100$ days) events to $A_V \sim 1.5$ mag, suggesting that these events are not caused by ever larger clumps. We propose that each long event consists of a series of events, or a continuous event, by clumps distributed along a string or a spiral arm. In this case, the duration gets longer, but the depth is not deeper.

The depth-duration relation of T Tauri stars has been discussed by Findeisen et al. (2013) with 3 yr monitoring of Palomar Transient Factory (PTF) for the North America Nebula complex. In their sample of 29 stars, there are fading events with a variety of depth (up to $\sim$ 2 mag) and duration (1–100 days). Stauffer et al. (2015), with a

high-cadence light curve from the *CoRoT* campaign for NGC 2264, identified YSO fading events up to 1 mag. Guo et al. (2018) summarized event parameters for different stars, including those in Stauffer et al. (2015), and found those with durations less than 10 days varied typically with a depth of ≤ 1 mag, whereas those lasting more than ~ 20 days have a roughly constant amplitude ~ 2–3 mag. All these studies made use of samples of different stars with a diverse star/disk masses, ages, inclination angles, etc., and no clear correlation was evidenced between depth and duration. In comparison, our investigation is for a single target with distinct correlations for the short and for the long events.

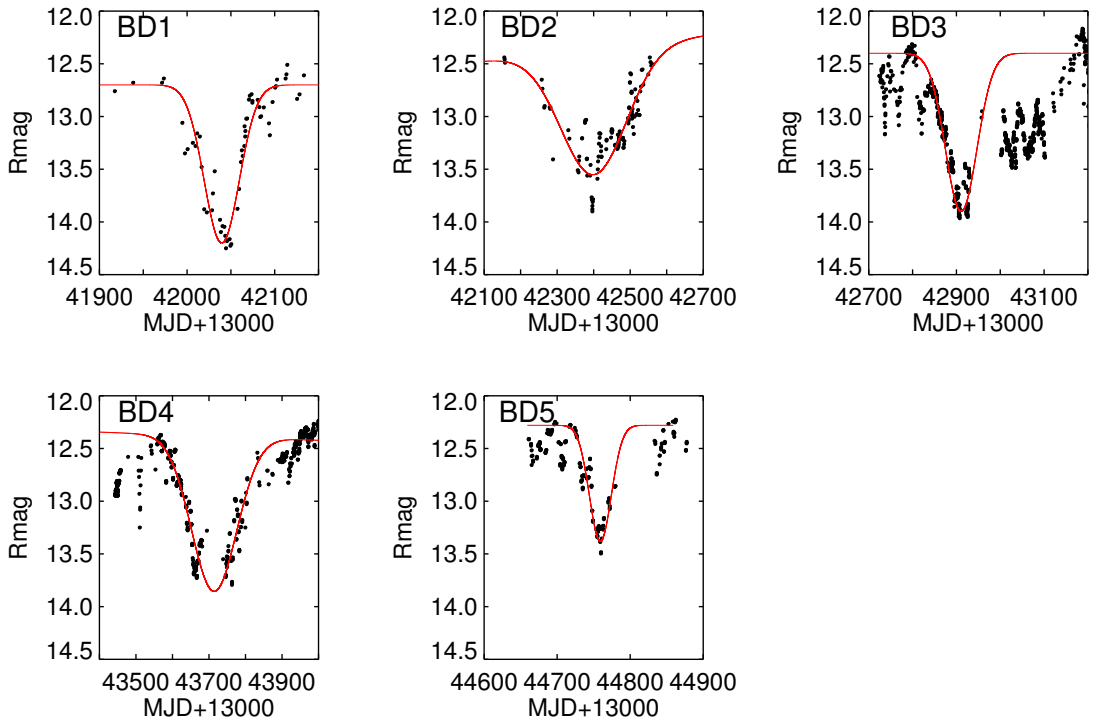


Figure 5. The Gaussian fitting to each of the major flux drop events.

3.2. *Color Variations*

Along with the light curves, Figure 1 also presents the $B-V$ color curve, i.e., the temporal variation. Figure 7a illustrates how the B magnitude of GM Cep varies with its $B-V$ color. In this color-magnitude diagram (CMD), GM Cep in general becomes redder when fainter, suggesting normal interstellar extinction/reddening. The slope of the reddening vector, marked by an arrow, is consistent with a total-to-selective extinction law of $R_V = 5$ (Mathis 1990), rather than with the nominal $R_V = 3$, implying larger dust grains than in the diffuse interstellar clouds. Between $B \sim 15.2$ mag and $B \sim 15.7$ mag, the extinction appears independent of the $(B-V)$ color, indicative of gray extinction by even larger grains (> 10 μm, (Eiroa et al. 2002). The trend is yet different toward the faint state; namely the color turns bluer when fainter. This color reversal, or the "bluing effect", has been known (Bibo & The 1990; Grinin et al. 1994; Grady et al. 1995; Herbst & Shevchenko 1999; Semkov et al. 2015), with the widely accepted explanation being that during the flux minimum, when direct star light is heavily obscured by circumstellar dust, the emerging light is dominated by forward scattered radiation into the field of view.

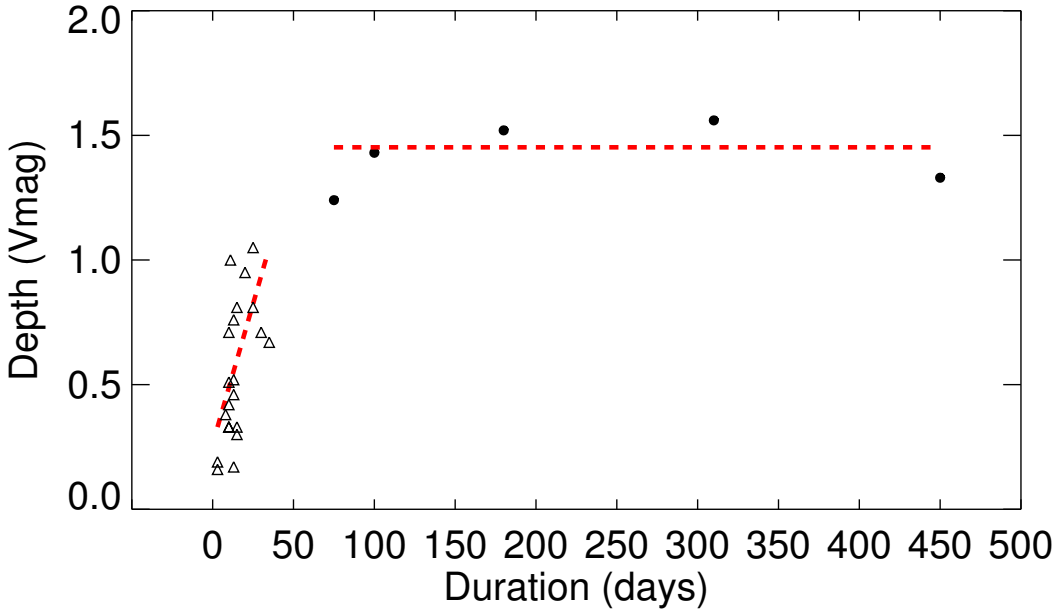


Figure 6. Depth versus duration of occultation events. Each event is parameterized by a Gaussian fit to the light curve as illustrated in Figure 5. There is a linear trend for short events (triangles), whereas for long events (circles) the extinction depth levels off.

The bluing phenomenon is also illustrated in Figure 1, where a few deep minima are marked, each by a thick red line, during which the corresponding color turns blue near the flux minimum. Additional CMDs in V versus $V-R$, and R versus $R-I$, where the data in I are adopted from those reported by Semkov et al. (2015), indicate also normal reddening in the bright state, whereas the bluing tends to subside toward longer wavelengths, in support of the scattering origin, as shown in Figure 7b.

3.3. *Polarization*

Figure 8 presents the linear polarization in r'-band of GM Cep, and of two comparison stars including one of the photometric reference stars and a field star. GM Cep displays a varying polarization with $P = 3\%$–8% but with an almost constant position angle of $\sim 72°$. The two comparison stars remain steadily polarized, each of $P \lesssim 2\%$ with a variation $\lesssim 1\%$.

Adding up the TRIPOL measurements at four polarizer angles gives the total flux. As seen in Figure 8, the TRIPOL r' light curve, albeit with lower cadence, allows for diagnosis of simultaneous photometric and polarimetric behavior. The broadband light curves in turn serve to indicate the overall brightness states at which the polarization data are taken.

Figure 9a plots the polarization in each band, $P_{g'}$, $P_{r'}$, and $P_{i'}$. The polarization exhibits a slowly varying pattern, declining from 6% to 9% in the fall of 2014 to 3%–5% in 2015 July/August, and reclining to 5% – 7% near the end of 2015. A similar pattern seems to exist also in 2017 but with a variation of 2% – 5%. At the same time, the slow brightness change in each case, notwithstanding abrupt flux drops, seems to have a reverse trend. In particular, the

Table 3. Flux Drop Events.

ID	MJD	Duration (days)	ΔB (mag)	ΔV (mag)	ΔR (mag)	(Remarks)
			Major Events			
BD01	55039	100	1.45	1.50	1.50	
BD02	55401	450	1.45	1.40	1.20	
BD03	55910	180	1.70	1.60	1.50	
BD04	56713	310	1.75	1.64	1.47	
BD05	57759	75	1.45	1.30	1.10	
			Minor Events			
SD01	55736	10	0.79	0.75	0.67	
SD02	55767	30	0.82	0.75	0.63	
SD03	55818	35	0.80	0.70	0.65	
SD04	56205	25	1.05	0.85	0.78	
SD05	56415	13	0.87	0.80	0.72	
SD06	56429	10	0.52	0.44	0.40	
SD07	56510	11	0.65	1.05	0.70	V includes AAVSO data
SD08	56553	15	0.37	0.32	0.30	
SD09	56763	13	0.35	0.55	0.68	
SD10	56784	13	0.55	0.48	0.48	
SD11	56865	13	-	0.40	-	
SD12	56944	13	0.33	0.18	0.20	
SD13	56972	3	0.22	0.17	0.15	
SD14	56989	3	0.22	0.20	0.18	
SD15	57184	8	0.49	0.40	0.36	
SD16	57263	25	1.10	1.10	1.40	incomplete sampling in B and V
SD17	57291	10	0.40	0.35	0.30	
SD18	57333	10	0.30	0.35	0.35	
SD19	57415	28	0.95	-	0.87	
SD20	57511	20	1.10	1.00	0.92	
SD21	57591	15	0.45	0.35	0.30	
SD22	57656	10	0.61	0.54	0.48	
SD23	57946	15	1.05	0.85	0.80	

smooth brightening in late 2014, where polarization data are densely sampled, is clearly associated with a monotonic decrease in polarization. A similar brightness-polarization pattern is seen from early 2017 to early 2018, for which the brightening and fading in the light curve is associated with a decreasing-turn-increasing trend in polarization.

Note that in general the polarization is higher at shorter wavelengths, but at certain epochs, particularly at flux minima, e.g., at the end of 2015 and the beginning of 2017, an "anomalous" wavelength dependence seems to emerge, so that the g' band becomes the least polarized.

4. THE CLUMPY DISK STRUCTURE IN GM CEP

The photopolarimetric measurements enable inference on the occultation configuration in a qualitative way. For example, a sequential blockage of the circumstellar environs and the star will result in a certain photometric and polarimetric behavior. The high-cadence light curves, furthermore, allow quantitative derivation of the depth, duration, etc., of the occulting body. We present the analysis and interpretation of both kinds in this section.

4.1. *Occultation Geometry Inferred By the Polarization Data*

The level of polarization at wavelength λ is defined as

$$P_\lambda(\%) = \frac{F^p_\lambda}{F^t_\lambda} = \frac{F^p_\lambda}{F^p_\lambda + F^u_\lambda} = \frac{1}{1 + F^u_\lambda / F^p_\lambda},$$

where F^t is the total flux, which is decomposed into polarized flux (F^p) and unpolarized flux (F^u), with $F^t = F^p + F^u$. At each observing epoch, P_λ and F^t are measured, therefore F^p and F^u can be derived. In general the starlight is not polarized, but the scattered light from the inner gaseous envelope/disk is, which is fainter and bluer in color than the direct starlight.

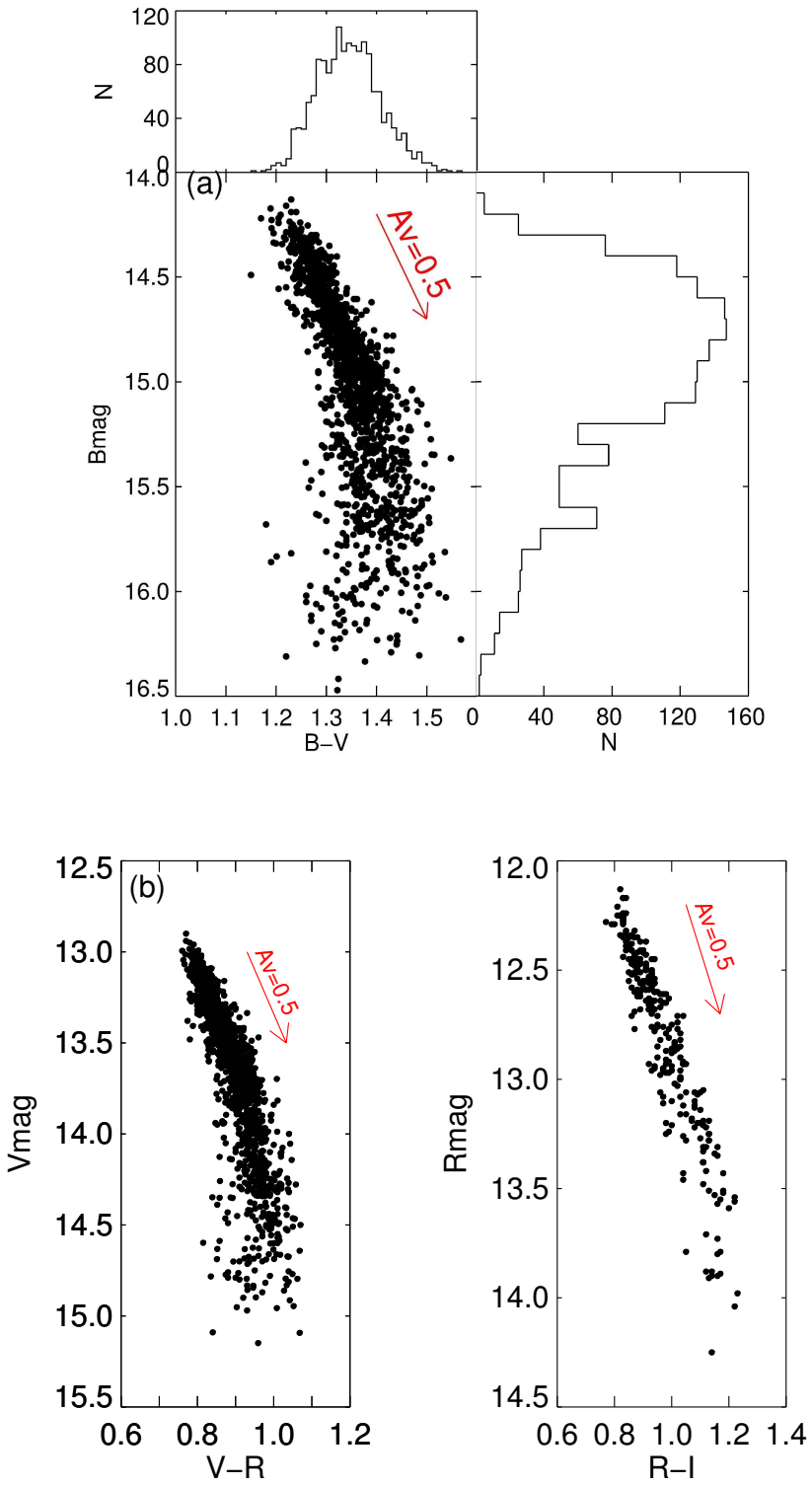


Figure 7. (a) The B magnitude versus $B-V$ color for GM Cep, using data in Figure 1. The panel on the right plots the histogram of the brightness in B, whereas the panel on the top plots the histogram of the $B-V$ color. The arrow marks the reddening vector for $A_V = 0.5$ mag assuming a total-to-selective extinction of $R_V = 5.0$. (b) The same as in (a) but for V versus $V-R$ and R versus $R-I$.

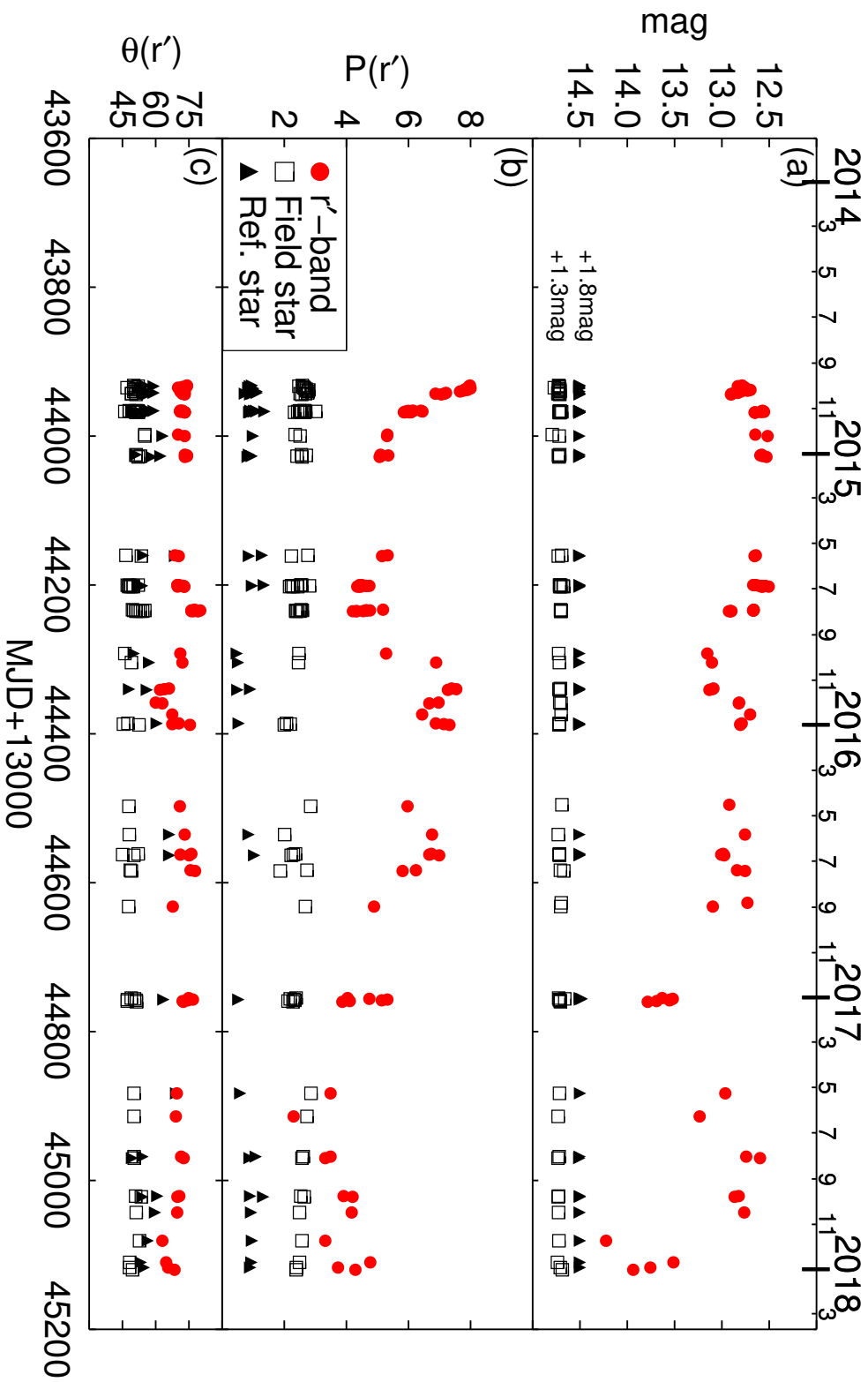


Figure 8. (a) The r'-band light curve (in black) for GM Cep, together with one of the photometric reference stars (filled triangles) and one field star (squares), in the same field of images. (b) The changing polarization level of GM Cep, in comparison to the two comparison stars. (c) The polarization angle for GM Cep remaining steady (72°) during three years of monitoring.

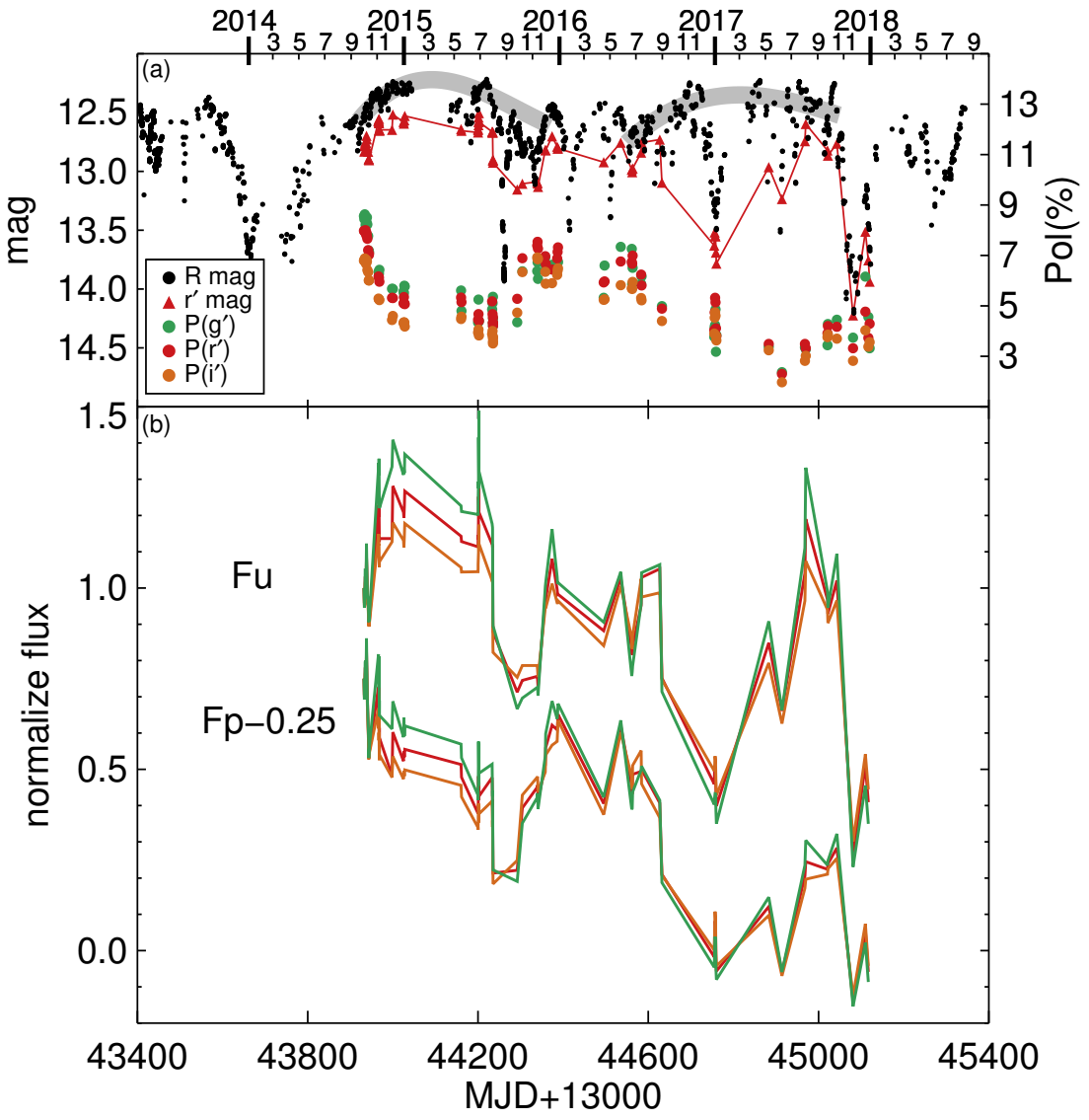


Figure 9. (a) The photopolarimetric r'-band light curve (in red) vs. the R-band light curve (in black), and shown below the polarization levels in g' (in green), r' (in red), and i' (in brown). The gray shades represent the slow brightness changes and simultaneous behavior of the polarization. (b) The light curves for unpolarized flux (F^u) and polarized flux (F^p), with the same color symbols as in (a).

The temporal variations of F^p_λ, F^u_λ, and F^t_λ, plus the wavelength dependence of these variations, provide clues on the geometry of a clump, or a string of clumps, relative to the stellar system (star plus disk). The last part of the equation suggests that (1) if F^u_λ remains the same, P_λ changes with F^p_λ in the sense that as F^p_λ decreases, so does P_λ. The dust reddening by occultation makes this dependence stronger at shorter wavelengths. But (2) if F^u_λ changes, because it dominates the brightness over F^p_λ, so, for example, as F^u_λ decreases, P_λ increases.

Figure 9b exhibits how the decomposed polarized (F^p) and unpolarized (F^u) components vary, respectively, at different wavelengths. To facilitate the comparison, each curve is scaled to its first data point to demonstrate the relative level of flux changes. The decomposition makes it clear that the decreasing polarization near the end of 2014, with $P_{g'} > P_{r'} > P_{i'}$ (see Fig. 9a), corresponding to the brightening of the star system, is the result of a fading F^p_λ alongside with a brightening F^u_λ, as evidenced in Fig. 9b, both leading to a decreasing P_λ in every wavelength. In the occultation scenario, the star system would be just coming out of a major event, and during such an egress, the clump was unveiling the star and blocking a progressively larger part of the envelope. Incidentally the deep flux drop event at the beginning of 2017 has polarization measured. At the brightness minimum, the level of polarization changes little, but with the anomaly $P_{r'} > P_{i'} > P_{g'}$. Inspection of the decomposition result reveals that both F^u_λ and F^p_λ decline to almost an all-time low, particularly at shorter wavelengths. This is the configuration when the star and the envelope are both heavily obscured.

On YSO photometric and polarimetric variability, Wood et al. (1996) and Stassun & Wood (1999) modeled the rotationally modulated multiwavelength photopolarization due to scattering of light by stellar hot spots, under different simulation parameters, such as the size and latitude of the hot spot, inclination, truncation radius, and geometry (e.g., flat or flared) of the disk. In general, the simulations suggested an amplitude of polarization variability less than about 1%. The polarization variability due to a warped disk is similarly low, as demonstrated in the case of AA Tau, a prototype of dippers, with a variation of $\sim 0.5\%$ in the V-band during the occultation O'Sullivan et al. (2005).

Recent modeling by Kesseli et al. (2016) of the photopolarimetric variability of YSOs plus accretion disks considered the spot temperature, radius of inner disk, structure, and inclination of the warp disk. Only star and dust emission was included, with no gas emission, but still, the typical polarization is expected to vary by less than $\sim 1\%$. It is interesting that the polarization level of I-band normally is always higher than that of the V-band, consistent with the wavelength dependence of our observations, albeit with limited time coverage, near flux minima. Hot starspots or a warped inner disk alone apparently cannot account for the large polarization variability seen in GM Cep. An additional gaseous envelope likely plays an important role.

4.2. *Clump Parameters By the Light-curve Analysis*

The long-term light curves render conclusive evidence that the major flux drops detected in GM Cep are caused by occultation of the young star and the envelope by circumstellar dust clumps. These dust grains are large in size, inferred by the reddening law (see §3.2), and distributed in a highly nonuniform manner. This density inhomogeneity could signify the protoplanetary disk evolution in transition from grain growth (of μm size) to planetesimal formation (of kilometer size) (Chen et al. 2012).

Accretion plus viscous dissipation heats up a young stellar disk early on. As the accretion subsides and grains get clumpy, the disk becomes passive, in the sense that the dust absorbs starlight, warms up, and reradiates in infrared (Chiang & Goldreich 1997). The frequent occultation events imply a geometry that would have led to a significant stellar extinction and a flat spectral energy distribution (SED). Instead, however, because of the grain coagulation, GM Cep (1) has a moderate $A_V = 2$–3 mag, partly of interstellar origin, despite the copious dust content evidenced by the elevated fluxes in far-infrared and submillimeter wavelengths (Sicilia-Aguilar et al. 2008), and also (2) has an SED characteristic of a T Tauri star (Sicilia-Aguilar et al. 2008) with a noticeable infrared excess. In a passive disk, hydrostatic equilibrium results in a structure to flare outward (Kenyon & Hartmann 1987; Chiang & Goldreich 1997), so the dust intercepts more starlight than a geometrically thin disk.

Ring- or spiral-like structure in YSO disks seems ubiquitous, as evidenced by, e.g., recent ALMA imaging in molecular lines or in continuum of the Herbig Ae/Be star AB Aur (Tang et al. 2012, 2017), the class II object Elias 2-27 (Pérez et al. 2016), or by HiCIAO/Subaru polarimetric imaging of FUors (Liu et al. 2016). Such a structure may be induced by a planet companion (Zhu et al. 2015) or by gravitational instability (Kratter & Lodato 2016). All these rings or spirals have some tens to hundreds of astronomical units in extents.

The most enlightening finding relevant to our work is the detection in the T Tauri star HL Tau at 7 mm of a distribution of clumps along the main ring of thermalized dust found earlier by at shorter wavelengths, where large

grains reside (Carrasco-González et al. 2016, see their Figure 2). The most prominent one, at $\sim 0\farcs1$ from the star, or ~ 14 au at a distance of 140 pc, with an estimated mass of 3–8 $M_\oplus$, is considered by these authors as a possible planetary embryo.

We have no knowledge of the location of the (strings of) clumps in the GM Cep disk, or of their geometric shape. But we present the following exercise, using theoretical disk models, to shed light on the possible constraints on clump parameters. The largest clumps in GM Cep, as seen in Figure 6, cause a maximal extinction of $A_V^c = 1.5$ mag with a time scale of ~ 50 days. Note that here A_V^c refers to the extinction caused by the occultation of the clump, to be distinguished from the interstellar plus circumstellar extinction of the star. The maximal extinction provides information on the column density of dust, and the duration time on the scale of the clump. The fiducial disk by Chiang & Goldreich (1997) adopts a stellar temperature $T_* = 4000$ K, mass $M_* = 0.5\ M_\odot$, and radius $R_* = 2.5\ R_\odot$. With veiling and line blending due to fast rotation, the spectral type of GM Cep is uncertain, ranging from an F9 (Huang et al. 2013) to G5/K3 (Sicilia-Aguilar et al. 2008). In any case the star is hotter (with higher pressure) but more massive (with stronger gravitational pull), and the hydrostatic conditions in the disk turn out to be similar. This means the disk height (H) is scaled with the radius (r) $H/r \approx 0.17(r/\mathrm{au})^{2/7}$ (Chiang & Goldreich 1997). A clump at $r = 14$ au thus would subtend an opening angle (viewing the rim from the star) of $\sim 20°$; at $r = 1$ au, the angle would become $\sim 10°$, for which the disk has to be close to edge-on for occultation to take place. Assuming 2 $M_\odot$ for GM Cep, a clump at 4–14 au has a projected Keplerian speed up to 11 km s^{-1}. So for a clump to traverse the GM Cep system, the linear size would be 0.3 au for $r = 14$ au. In the case $r = 1$ au, the orbital speed is faster, so the linear scale would be 1.2 au.

Alternatively, the clumps may be located closer in to the central star. The disk may not be monotonically flared, as the innermost disk is irradiated by starlight, and dust evaporation at temperature $T_{\rm evap} \sim 1500$ K results in an inner hole, hence an inner rim or "wall" in the flaring disk, which accounts for the bump near 2–3 μm observed in the SEDs of some YSOs (Dullemond et al. 2001; Eisner et al. 2004). This temperature corresponds to a distance from the central star, $r_{\rm rim} = (L_*/4\pi T_{\rm rim}^4\sigma)^{1/2}(1+(H_{\rm rim}/r_{\rm rim}))^{1/2}$, where L_* is the luminosity of the star, $T_{\rm rim} = T_{\rm evap}$ is the temperature at the rim, $H_{\rm rim}$ is the vertical height of the inner rim, and σ is the Stefan–Boltzmann constant (Dullemond et al. 2001). Given $L_* = 26\ L_\odot$ for GM Cep (Sicilia-Aguilar et al. 2008), adopting $H_{\rm rim}/r_{\rm rim} = 0.2$ (Dullemond et al. 2001), the estimated inner rim radius is roughly $r_{\rm rim} \sim 0.4$ au, corresponding to an opening angle $\arctan(H_{\rm rim}/r_{\rm rim}) \sim 11°$. Even though the chance of occultation is higher with a clump closer to the star, a faster Keplerian speed would lead to a linear size of 1.7 au. We conclude that the "clump," or the region of density enhancement in the disk has a length scale up to roughly 0.1–1 au cross the line of sight.

The depth, or the length scale along the line of sight, is related to the maximum $A_V^c = 1.5$ mag, or the column density of dust. Integration requires detailed disk structure, such as the vertical and radial density profiles, grain size distribution, midplane settling, etc. Such a complexity is beyond the scope of this paper and in fact not justified by our data. Here we again attempt to gain some physical insights on the clump properties.

For a uniform disk, the volume mass density of dust $m_d = (N_d/\ell)\, M_{\rm grain}$, where N_d is the column density of dust, ℓ is the length of the sightline through the dusty medium, and $M_{\rm grain}$ is the mass of each grain. Each term is evaluated as follows.

The column density N_d is related to the extinction: $A_V^c = 1.086\tau_V = N_d\sigma_d Q_{\rm ext}$, where τ_V is the optical depth at V-band, $\sigma_d = \pi a^2$ is the geometric cross section of each (assuming spherical) grain of radius a, and $Q_{\rm ext}$ is the optical extinction coefficient, which, for grains large in size compared to the wavelength ($2\pi a >> \lambda$), $Q_{\rm ext} \approx 2$ (Spitzer 1978; van de Hulst 1957). Therefore, $N_d = 1.6\times10^5\ A_V^c\ [10\ \mu\mathrm{m}/a]^2$ cm^{-2}, and for each dust grain, assuming a material bulk density of 2 g cm^{-3}, the mass is $M_{\rm grain} = 8.4\times10^{-9}[a/10\mu\mathrm{m}]^3$ g. Given a gas density n_g, and a nominal gas-to-dust mass ratio of 100, $m_d = n_g m_H/100$, and so

$$\ell = \frac{5.4\times10^9}{n_g}\, A_V\, (\frac{a}{10\ \mu\mathrm{m}}) \quad [\mathrm{au}].$$

For GM Cep, $A_V^c = 1.5$ mag, and adopting a gas density $n_g = 10^{10}$ (Barrière-Fouchet et al. 2005), $\ell \sim 0.8$ au for $a = 10$ μm grains. For truly large grains, such as $a = 1$ mm, the extinction efficiency becomes much smaller, thus ℓ 100 times longer, to $\ell \sim 80$ au.

Admittedly, none of the simple assumptions we have made in the estimation is likely valid. Still, it is assuring that both the crossing time and the flux drop of occultation by a dust clump could end up with reasonable solutions, namely a region tens of astronomical units across in the young stellar disk, perhaps in a ring or a spiral configuration

located tens of astronomical units from the star, consisting of primarily 10 μm grains or larger. Given the overall low extinction of the star, small grains likely exist but not in quantity, as they had been agglomerated into large bodies.

5. CONCLUSION

Optical photometric and polarimetric monitoring of the UX Ori star GM Cep for nearly a decade reveals variations in brightness and in polarization of different amplitude and time scales. The essential results of our study are:

- GM Cep exhibits (1) brightness fluctuations $\lesssim 0.05$ mag on time scales of days, due partly to rotational modulation by surface starspots with a period of 3.43 days, and partly to accretion activity; (2) minor flux drops of amplitude 0.2–1.0 mag with duration of days to weeks; and (3) major flux drops up to 2.5 mag, each lasting for months, with a recurrent time, but not exactly periodic, of about 2 years.
- The flux drops arise from occultation of the star and gaseous envelope by orbiting dust clumps of various sizes.
- The star experiences normal dust reddening by large grains, i.e., the star becomes redder when fainter, except at the brightness minimum during which the star turns bluer when fainter.
- The maximum depth of an occultation event is proportional to the duration, about 1 mag per 30 days, for the events lasting less than ~ 50 days, a result of occultation by clumps of varying sizes. For the events longer than about 100 days, the maximum depth is independent of the duration and remains $A_V \sim 1.5$ mag, a consequence of transiting strings or layers of clumps.
- The $g'r'i'$ polarization levels change between 3% and 8%, and vary inversely with the slow brightness change, while the polarization angle remains constant. The polarization is generally higher at shorter wavelengths, but at flux minima, there is a reversal of wavelength dependence, e.g., the g'-band becomes the least polarized. Temporal variations of polarization versus brightness, once the total light is decomposed into polarized and unpolarized components, allow diagnosis of the occultation circumstances of the dust clumps relative to the star and envelope.
- Our data do not provide direct information on the size or location of the clumps, but the duration of an occultation sets constraints on the transverse size scale of the clump, while the maximum extinction depth is a measure of the column density of dust, hence a dependence of the line-of-sight length through the dusty medium. It is possible that GM Cep is an edge-on manifestation of the ring- or spiral-like structures found recently in young stars with imaging in infrared of scattered light, or in submillimeter of dust emission.

The NCU group acknowledges the financial support of the grants MOST 106-2112-M-008-005-MY3 and MOST 105-2119-M-008-028-MY3. We greatly thank the Jena group H. Gilbert, T. Zehe, T. Heyne, A. Pannicke, and C. Marka for kindly providing us with their efforts on acquiring data from Jena Observatory, which is operated by the Astrophysical Institute of the Friedrich-Schiller-University. Furthermore, we would like to thank the Thuringian State (Thüringer Ministerium für Bildung, Wissenschaft und Kultur) in project number B 515-07010 for financial support. The work by the Xinjiang Observatory group was in part supported by the program of the Light in China's Western Region (LCWR, grant No. 2015-XBQN-A-02) and National Natural Science Foundation of China (grant No. 11661161016). J. Budaj, Z. Garai, and T. Pribulla acknowledge VEGA 2/0031/18 and APVV 15-0458 grants as well as V. Kollar, J. Lopatovsky, N. Shagatova, S. Shugarov, and R. Komzik for their help with some observations. This research has made use of the International Variable Star Index (VSX) database, operated at AAVSO, Cambridge, Massachusetts, USA. We thank the referee for constructive comments that greatly improve the quality of the paper.

REFERENCES

Alcalá, J. M., Manara, C. F., Natta, A., et al. 2017, A&A, 600, A20

Barrière-Fouchet, L., Gonzalez, J.-F., Murray, J. R., Humble, R. J., & Maddison, S. T. 2005, A&A, 443, 185

Bibo, E. A., & The, P. S. 1990, A&A, 236, 155

Blinova, A. A., Romanova, M. M., & Lovelace, R. V. E. 2016, MNRAS, 459, 2354

Bouvier, J., Chelli, A., Allain, S., et al. 1999, A&A, 349, 619

Bouvier, J., Grankin, K. N., Alencar, S. H. P., et al. 2003, A&A, 409, 169
Bouvier, J., Grankin, K., Ellerbroek, L. E., Bouy, H., & Barrado, D. 2013, A&A, 557, A77
Briceño, C., Hartmann, L., Hernández, J., et al. 2007, ApJ, 661, 1119
Carrasco-González, C., Henning, T., Chandler, C. J., et al. 2016, ApJL, 821, L16
Chen, W. P., Hu, S. C.-L., Errmann, R., et al. 2012, ApJ, 751, 118
Chiang, E. I., & Goldreich, P. 1997, ApJ, 490, 368
Cody, A. M., & Hillenbrand, L. A. 2010, ApJS, 191, 389
Cody, A. M., Stauffer, J., Baglin, A., et al. 2014, AJ, 147, 82
Contreras, M. E., Sicilia-Aguilar, A., Muzerolle, J., et al. 2002, AJ, 124, 1585
Dullemond, C. P., Dominik, C., & Natta, A. 2001, ApJ, 560, 957
Eiroa, C., Oudmaijer, R. D., Davies, J. K., et al. 2002, A&A, 384, 1038
Eisner, J. A., Lane, B. F., Hillenbrand, L. A., Akeson, R. L., & Sargent, A. I. 2004, ApJ, 613, 1049
Errmann, R., Neuhäuser, R., Marschall, L., et al. 2013, Astronomische Nachrichten, 334, 673
Findeisen, K., Hillenbrand, L., Ofek, E., et al. 2013, ApJ, 768, 93
Fritzewski, D. J., Kitze, M., Mugrauer, M., et al. 2016, MNRAS, 462, 2396
Gaia Collaboration, Brown, A. G. A., Vallenari, A., et al. 2018, arXiv:1804.09365
Garai, Z., Pribulla, T., Hambálek, Ľ., et al. 2016, Astronomische Nachrichten, 337, 261
Giannini, T., Munari, U., Lorenzetti, D., et al. 2018, Research Notes of the American Astronomical Society, 2, 124
Goldreich, P., & Ward, W. R. 1973, ApJ, 183, 1051
Grady, C. A., Perez, M. R., The, P. S., et al. 1995, A&A, 302, 472
Grinin, V. P., The, P. S., de Winter, D., et al. 1994, A&A, 292, 165
Grinin, V. P., Rostopchina, A. N., & Shakhovskoi, D. N. 1998, Astronomy Letters, 24, 802
Gullbring, E., Hartmann, L., Briceño, C., & Calvet, N. 1998, ApJ, 492, 323
Guo, Z., Herczeg, G. J., Jose, J., et al. 2018, ApJ, 852, 56
Hamilton, C. M., Herbst, W., Shih, C., & Ferro, A. J. 2001, ApJL, 554, L201
Hartmann, L., & Kenyon, S. J. 1985, ApJ, 299, 462
Herbig, G. H. 1989, European Southern Observatory Conference and Workshop Proceedings, 33, 233
Herbst, W., Herbst, D. K., Grossman, E. J., & Weinstein, D. 1994, AJ, 108, 1906
Herbst, W., & Shevchenko, V. S. 1999, AJ, 118, 1043
Hillenbrand, L. A. 2008, Physica Scripta Volume T, 130, 014024
Huang, P.-C., Chen, W.-P., Hu, C.-L., et al. 2018, Bulletin de la Societe Royale des Sciences de Liege, 87, 145
Huang, Y. F., Li, J. Z., Rector, T. A. & Mallamaci, C. C. 2013, AJ, 145, 126
Johansen, A., Oishi, J. S., Mac Low, M.-M., et al. 2007, Nature, 448, 1022
Kearns, K. E., & Herbst, W. 1998, AJ, 116, 261
Kenyon, S. J., & Hartmann, L. 1987,ApJ, 323, 714
Kesseli, A. Y., Petkova, M. A., Wood, K., et al. 2016, ApJ, 828, 42
Kratter, K., & Lodato, G. 2016, ARA&A, 54, 271
Küker, M., Rüdiger, G., & Kitchatinov, L. L. 2011, A&A, 530, A48
Kun, M. 1986, Information Bulletin on Variable Stars, 2961, 1
Liu, H. B., Takami, M., Kudo, T., et al. 2016, Science Advances, 2, e1500875
Lomb, N. R. 1976, Ap&SS, 39, 447
Mamajek, E. E., Meyer, M. R., Hinz, P. M., et al. 2004, ApJ, 612, 496
Marschall, L. A., Karshner, G. B., & Comins, N. F. 1990, AJ, 99, 1536
Mathis, J. S. 1990, ARA&A, 28, 37
Mercer, E. P., Miller, J. M., Calvet, N., et al. 2009, AJ, 138, 7
Monet, D. G., Levine, S. E., Canzian, B., et al. 2003, AJ, 125, 984
Morgenroth, O. 1939, Astronomische Nachrichten, 268, 273
Munari, U., Castellani, F., Giannini, T., et al. 2017, Atel#11004
Mugrauer, M., & Berthold, T. 2010, Astronomische Nachrichten, 331, 449
Mugrauer, M. 2016, Astronomische Nachrichten, 337, 226
Natta, A., Testi, L., Muzerolle, J., Randich, S., Comerón, F., & Persi, P. 2004, A&A, 424, 603
Natta, A., Testi, L., Calvet, N., et al. 2007, Protostars and Planets V, eds. B. Reipurth, D. Jewitt, and K. Keil, University of Arizona Press, Tucson, 767
Neuhäuser, R., Errmann, R., Berndt, A., et al. 2011, Astronomische Nachrichten, 332, 547
O'Sullivan, M., Truss, M., Walker, C., et al. 2005, MNRAS, 358, 632
Patel, N. A., Goldsmith, P. F., Snell, R. L., Hezel, T., & Xie, T. 1995, ApJ, 447, 721

Pérez, L. M., Carpenter, J. M., Andrews, S. M., et al. 2016, Science, 353, 1519

Raetz, S., Schmidt, T. O. B., Czesla, S., et al. 2016, MNRAS, 460, 2834

Rodriguez, J. E., Pepper, J., Stassun, K. G., et al. 2015, AJ, 150, 32

Rodriguez, J. E., Reed, P. A., Siverd, R. J., et al. 2016, AJ, 151, 29

Romanova, M. M., Ustyugova, G. V., Koldoba, A. V., & Lovelace, R. V. E. 2013, MNRAS, 430, 699

Rostopchina, A. N., Grinin, V. P., & Shakhovskoi, D. N. 1999, Astronomy Letters, 25, 243

Safronov, V. S. 1972, Evolution of the protoplanetary cloud and formation of the earth and planets., by Safronov, V. S.. Translated from Russian. Jerusalem (Israel): Israel Program for Scientific Translations, Keter Publishing House, 212 p.,

Scargle, J. D. 1982, ApJ, 263, 835

Schmidt, G. D., Elston, R., & Lupie, O. L. 1992, AJ, 104, 1563

Schulz, R., Erd, C., Guilbert-Lepoutre, A., et al. 2014, AAS/Division for Planetary Sciences Meeting Abstracts #46, 46, 214.05

Semkov, E. H., & Peneva, S. P. 2012, Ap&SS, 338, 95

Semkov, E. H., Ibryamov, S. I., Peneva, S. P., et al. 2015, PASA, 32, e011

Sicilia-Aguilar, A., Hartmann, L. W., Briceño, C., Muzerolle, J., & Calvet, N. 2004, AJ, 128, 805

Sicilia-Aguilar, A., Hartmann, L. W., Hernández, J., Briceño, C., & Calvet, N. 2005, AJ, 130, 188

Sicilia-Aguilar, A., Hartmann, L. W., Fürész, G., et al. 2006, AJ, 132, 2135

Sicilia-Aguilar, A., Hartmann, L. W., Calvet, N., et al. 2006, ApJ, 638, 897

Sicilia-Aguilar, A., Merín, B., Hormuth, F., et al. 2008, ApJ, 673, 382

Spitzer, L. 1978, Physical processes in the interstellar medium, Wiley, New York

Stassun, K., & Wood, K. 1999, ApJ, 510, 892

Stauffer, J., Cody, A. M., McGinnis, P., et al. 2015, AJ, 149, 130

Strassmeier, K. G. 2009, A&A Rv, 17, 251

Suyarkova, O. G. 1975, Peremennye Zvezdy, 20, 167

Tang, Y.-W., Guilloteau, S., Piétu, V., et al. 2012, A&A, 547, A84

Tang, Y.-W., Guilloteau, S., Dutrey, A., et al. 2017, ApJ, 840, 32

Terquem, C., & Papaloizou, J. C. B. 2000, A&A, 360, 1031

van de Hulst, H. C. 1957, Light Scattering by Small Particles, Dover, New York

Watanabe, M., Takahashi, Y., Sato, M., et al. 2012, Proc. SPIE, 8446, 84462O

Weidenschilling, S. J. 2000, SSRv, 92, 295

Wood, K., Kenyon, S. J., Whitney, B. A., & Bjorkman, J. E. 1996, ApJL, 458, L79

Xiao, L., Kroll, P., & Henden, A. A. 2010, AJ, 139, 1527

Zhu, Z., Dong, R., Stone, J. M., & Rafikov, R. R. 2015, ApJ, 813, 88